buildings

MDPI

Article

Quantification of Moment–Rotation Relationship of Monolithic Precast Beam–Column Connections

Baoxi Song, Weizhi Xu *, Dongsheng Du and Shuguang Wang

College of Civil Engineering, Nanjing Tech University, Nanjing 211816, China; songbaoxi77@outlook.com (B.S.); ddshy@njtech.edu.cn (D.D.); wsg@njtech.edu.cn (S.W.)

* Correspondence: xuwz@njtech.edu.cn

Abstract: The accurate prediction of nonlinear structural behaviors under different seismic intensities is an important basis for seismic resilience assessments of building structures. The moment–rotation relationship is often used to characterize the seismic performance of connections, and is widely used in high-efficiency nonlinear structural analysis. In this paper, a method of calculating the curve using a four-linear equivalent model is presented, aiming to quantify the characteristic point parameters of the moment–rotation curves of monolithic precast beam–column (MPBC) connections for engineering design purposes. The method considered the contribution of the elastic flexure of beams and columns, the relative slip of beam longitudinal bars in the core zone, and the formation of plastic hinges at beam ends to the total deflection. Due to the presence of local complex configurations in MPBC connections, the fine fiber section method was used for moment–curvature analysis of critical beam sections. The determination of the sectional analysis processes was controlled by the strain of steel bars or concrete or their coupling effect. In addition, a two-step method was proposed to construct the moment–rotation relationship of cruciform beam–column connections for solving the deformation compatibility of beams on both sides of the column caused by asymmetric reinforcement and the strength difference between new and old concrete. To reflect the current manufacturing level of MPBC connections, 58 representative specimens reported in recent years were analyzed and classified as type 1–5. All types of MPBC connections and their 18 cast-in situ counterparts were calculated using the proposed method for both verification and quantification. The verification showed that the proposed method had good applicability to both cast-in situ and precast beam–column connections. The quantification showed that the characteristic point parameters were slightly different between these two connections. Accordingly, modification coefficients were suggested for MPBC connections to facilitate design.

Keywords: seismic resilience; moment–rotation curve; monolithic precast; beam–column connection; quantification

check for updates

Citation: Song, B.; Xu, W.; Du, D.; Wang, S. Quantification of Moment–Rotation Relationship of Monolithic Precast Beam–Column Connections. *Buildings* **2022**, *12*, 11. https://doi.org/10.3390/buildings12010011

Academic Editor: Alessandra Aprile

Received: 29 November 2021
Accepted: 21 December 2021
Published: 24 December 2021

1. Introduction

In recent years, due to the encouragement of the government, monolithic precast frame structures have been vigorously applied in China. However, the difference of nonlinear behavior between cast-in-place and precast structures has not received attention in design and seismic resilience assessments. The determination of the structural damage state is an important part in the seismic resilience assessment of buildings, which is also the basis for the calculation of repair cost, building repair time, and casualties. Therefore, it is necessary to investigate the force state of the connections under different deformations for scientifically evaluating the seismic resilience of monolithic precast frame structures. The moment–rotation relationship is an intuitive reflection of the mechanical behaviors of concrete members or their subassemblies, which includes the fundamental performance parameters, i.e., initial stiffness, load-carrying capacity, ductility, and nondestructive displacement. Additionally, the cumulative energy dissipation capacity of members relies on their ductility, and thus can be indirectly compared to the moment–rotation relationship when the hysteresis curve shows no obvious pinch effect. The moment–rotation curve can be utilized for the rapid definition of the nonlinearity of concrete members. Therefore, it is widely adopted by commercial analysis software and is preferred by engineering designers. Reliable structural nonlinear analysis results can be obtained if the moment–rotation relationship of the components can be accurately predicted.

The precast concrete structure is a product of the progress of modern industrialization. Its development is of great significance to improve building quality, environment protection, and intelligent construction level. The construction process of a monolithic precast frame basically goes through three stages: component factory processing, transportation, and field assembly. The basic components of the frame (e.g., beams, columns, slabs) are divided into individual members to be manufactured and cured in the component factory. After the members reach the construction strength, they can be transported to the site and assembled in order. Since the prefabricated members can withstand the construction loads during the assembly stage, the use of scaffolding is reduced to a certain extent. Some self-sustaining measures, such as thickened beam U-shells, corbels or a temporary steel angles arrangement, and diagonal bracing bars in the core zone, also meet this purpose [1–3]. During on-site construction, the members are integrated by a reliable connection of reinforcements and post-poured concrete. Therefore, the connection between prefabricated members becomes the key link for the quality control of frame structures. Among these connections, column–foundation connections and beam–column connections are two parts that determine the structural safety. Column–foundation connections are generally achieved by sleeve grouting, and have been extensively used in engineering. In tensile tests of grouted sleeves, the steel bars usually fracture outside the sleeves [4,5], and the reliability of such a connection has also been confirmed in relevant joint tests [6]. By contrast, beam–column connections are of diverse configurations, and have more options in the location of the post-casting area, the connection and anchorage methods of the steel bars, the treatment of the concrete-connecting interface, the type of bars and concrete, the usage of special materials, and other aspects. Therefore, some scholars remain in search of the possibility of improving their performance [7–9]. Since the design strategy of MPBC connections is to emulate cast-in situ connections, the original calculation methods are used in their usual design [10], except for the additional structural measures [11]. There is an urgent need to understand the differences between the emulated connections and cast-in situ connections in bearing capacity and deformability, because these differences will affect the seismic performance of the whole structure. Both of the two aspects are included in the moment–rotation curves. Therefore, it is quite necessary to quantify them.

At present, analysis methods for the moment–rotation relationship of cast-in situ beam–column connections have been reported [12,13]. The results of the used methods were verified with the data from completed tests and empirical modifications were given for the general application of these methods. Considering the shear failure of existing bridge piers constructed in accordance with old codes, a flexure–shear interaction numerical model was proposed [14]. The model explained the different failure modes (ductile bending failure and brittle shear failure) of specimens caused only by different reinforcement ratios well. As for precast beam–column joints, a hybrid system developed by the PRESSS program, using unbonded post-tensioned tendons and mild steel for realizing self-centering and energy dissipation capabilities, has been tested and modeled [15,16]. The analytical model of parallel rotational springs representing the two moment contributors, respectively, proved satisfactory. However, there are few verifications for MPBC connections. On the one hand, the existing calculation methods are no longer applicable due to the diverse and complex local configurations of the above-mentioned MPBC connections. On the other hand, there is a lack of experimental foundations for the verification of calculating methods since relevant test reports have accumulated only in recent years.

The purpose of this paper is to propose a calculation method suitable for predicting the moment–rotation behaviors of MPBC connections based on the calculation concept of the traditional cast-in situ connections. A large number of test results, reported in recent years, were used as the database to quantify the moment–rotation relationship of MPBC connections. On this base, modification coefficients were given to provide a reference for relevant engineering designs.

2. Proposed Method

A common method for simplifying the moment–rotation curve or force–displacement curve is the adoption of a multi-fold line. In general, the tri-linear model has been able to reflect the nonlinearity of members approximately, and is extensively used [17]. In this paper, the four-linear model was adopted [18]. By adding an elastic limit control point (point A in Figure 1) before the yielding of the member, the elastic stiffness information can be expressed more accurately. This is helpful when evaluating the initial damage of the components. Figure 1 shows the force–deformation feature of a typical cruciform beam–column joint and the idealization of its positive moment–rotation curve. When the length of the upper and lower columns is the same, the maximum bending moment of the columns is half of the total. Points A–D on the dashed line are the cracking point, yield point, peak point, and ultimate point, respectively. Point A is at the position where stiffness deviates. Point C is the maximum moment point on the curve. Point B is the point of tangency of the parallel line of the origin to line C on the M–θ curve. This is commonly named the farthest point method, and its effectiveness was confirmed in reference [19]. This definition approach is relatively objective and easy for machinery computation. Point D is generally considered the failure point of the connection. Through these definitions, an actual behavior can be idealized as a four-linear line; thus, the solution of the actual curve can be simplified as the calculation of characteristic point parameters (moment value and rotation value for each point).

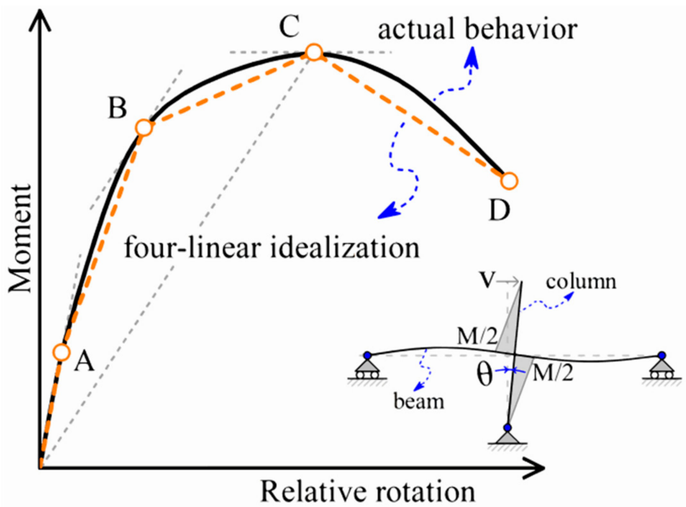

Figure 1. Idealization of moment–rotation relationship.

2.1. Calculation of Moment at Beam End

For a beam member, the moment at point A was deemed as the cracking moment $M_{\rm cr}$, and was calculated by the following formula:

$$M_{\rm cr} = \gamma f_{\rm t} W_0 \tag{1}$$

where, γ is the plastic influence coefficient of the sectional resistance moment, which can be calculated by $\gamma = (0.7 + 120/h_{\rm b})\gamma_{\rm m}$ [10]. Here, $h_{\rm b}$ is the beam depth, which was given the value of 400 mm when $h_{\rm b} < 400$ mm. For a rectangular section, 1.55 was adopted for the coefficient $\gamma_{\rm m}$. The $f_{\rm t}$ in Formula (1) is the tensile strength of concrete, and W_0 is the elastic resistance moment of the tensile edge. Figure 2 shows the concrete at the top side of the beam reaching its cracking strain, $\varepsilon_{\rm t}$. The steel bars were equivalent to the concrete sections at the same position. For the upper steel bars, the equivalent area $A_1 = (E_{\rm s}/E_{\rm c})A_{\rm s,top}$

was obtained by Formula (2), where E_s and E_c are the elastic modulus of steel bars and concrete, respectively, and $A_{s,top}$ is the sum of areas of the upper longitudinal bars. The area A_2 can be calculated by the same method. According to the equal static moment of the tension zone and the compression zone, Formula (3) can be obtained and used to calculate the neutral axis depth x. Then, the inertia moment I_0 of the section can be calculated by Formula (4). W_0 can be obtained by I_0 ($W_0 = I_0/(h_b - x)$). The same method can be used when the concrete at the lower side reaches its cracking strain.

$$A_{s,top}\varepsilon_{s,top}E_s = A_1\varepsilon_{s,top}E_c \tag{2}$$

$$\frac{1}{2}b_b x^2 + A_2(x - a_{s,bot})^2 = \frac{1}{2}b_b(h_b - x)^2 + A_1(h_b - x - a_{s,top})^2 \tag{3}$$

$$I_0 = \frac{1}{12}b_b{h_b}^3 + A_1(h_b - x - a_{s,top})^2 + A_2(x - a_{s,bot})^2 \tag{4}$$

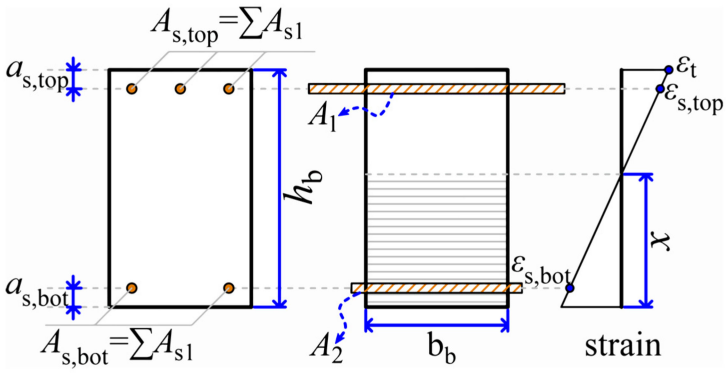

Figure 2. Equivalent section for calculating W_0 and its strain relationship.

The moment at point B was deemed as the yielding moment M_y, and the steel bars on the tensile side were considered yielding in the calculation. As shown in Figure 3, Formula (5) can be obtained by the deformation relationship. Thus, the strain of concrete and steel bars in the compression zone was correlated with the depth x of the compression zone. The stress–strain constitutive relationship of introduced concrete and steel bars is shown in Figure 4. Considering the confined effect of the stirrups, the modified Kent and Park stress–strain model was used for concrete [20,21], with the position of the centroids of the steel bars ($a_{s,top}$, $a_{s,bot}$ in Figure 2) as the boundaries of the confined concrete. The equivalent bilinear model was adopted for reinforcement, and the post-yield stiffness k_2 was 0.6% of the elastic stiffness k_1. Thus, the corresponding stresses $\sigma_{c,bot}$ and $\sigma_{s,bot}$ of the concrete and the steel bars in Figure 3 were obtained. Formula (6) can be derived by the equilibrium condition of the force in cross section, so as to find x. In the solution of integrals, the beam section was divided into 1 mm high fiber sections. When the solution accuracy was $x < 1$ mm, the section was considered to be in force equilibrium. This fine fiber section method is suitable for precast connections because it is convenient to consider the difference of concrete strength within the same section due to batch casting. M_y was calculated through Formula (7). In this process, the yield of longitudinal reinforcement was deemed as the only yield criterion of the whole beam.

$$\frac{\varepsilon_{c,bot}}{x} = \frac{\varepsilon_{s,bot}}{x - a_{s,bot}} = \frac{\varepsilon_y}{h_b - x - a_{s,top}} \tag{5}$$

$$\int_0^x \sigma_c b_b dx + \sigma_{s,bot}A_{s,bot} = f_y A_{s,top} \tag{6}$$

$$M = \sigma_{s,bot}A_{s,bot}(h_b - a_{s,top} - a_{s,bot}) + \int_0^x (h_b - a_{s,top} - x)\sigma_c b_b dx \tag{7}$$

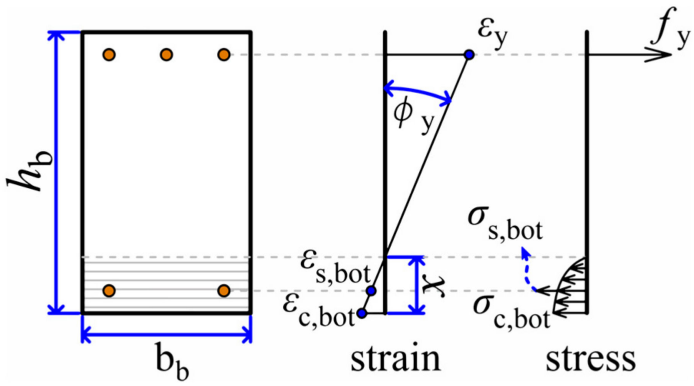

Figure 3. Stress and strain diagram of beam section when yielding.

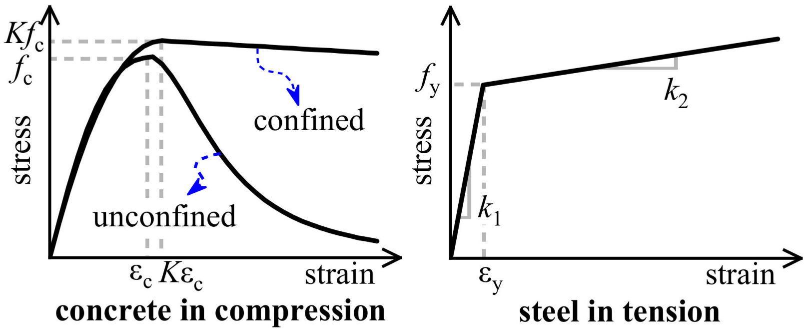

Figure 4. Simplified constitution of materials.

In the calculation of the peak moment M_p at point C, the strain of the steel bars at the tensile side of the beam was taken as a variable. For instance, the unidirectional tensile process of the upper steel bars was simulated approximately by the constant increase of $\varepsilon_{s,top}$ (ε_y deemed as the initial value); thus, a new equilibrium condition was formed and the depth x of the compression zone was solved by Formula (6). Then, the moment value at each equilibrium state was obtained by Formula (7), and M_p was the local maximum in the obtained M sequences, which ensured that the concrete at the compressed edge reached its peak strength. In this process, concrete strain was one of the criteria for terminating calculation.

The ultimate moment M_u at point D was controlled by the strain of concrete and reinforcement. When compressed concrete at the edge lost its strength (lower than 3 MPa) or the strain of tensile steel bars reached 0.06, the moment obtained was deemed as the ultimate moment. The two criterion conditions are relatively conservative, because point D is considered to be reached only when the strength of the connection decreases by 15%, or when there is a risk of subsequent loading in related tests, while, at that time, the protective concrete at the beam end has usually all spalling off. In addition, the steel bars, in accordance with the industry standard, will not fracture when the strain reaches 0.06 (the minimum guaranteed values for delivery inspection of ductility characteristics of reinforcement were given in Table 6 of code [22]). The moment value of point D can also be calculated by Formula (7).

2.2. Calculation of Column Rotation

The column rotation in this paper was contributed to by four mechanisms, namely, the elastic flexure of the beam, the relative slip of beam longitudinal bars in the core zone, the plastic hinge at the beam end, and the flexural deformation of the column (Figure 5). The design concept of "strong columns and weak beams, strong joints and weak members" was generally followed in the structural design, so the relative rotation caused by shear deformation in the core zone was ignored [12]. Rotation values generated by these mechanisms were identified as θ_1–θ_4.

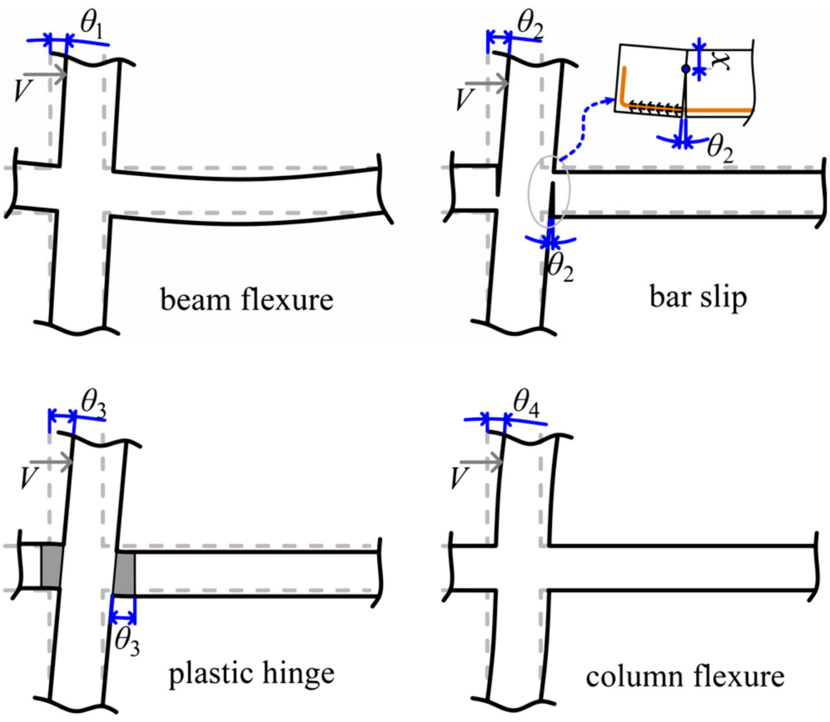

Figure 5. Four mechanisms contributing to column rotation.

The rotation value θ_1 was obtained by dividing the elastic deformation of the beam by its clear length l_b (Formula (8)), where M_b is the moment at the beam end, E is the elastic modulus of concrete, and I_b is the effective inertia moment of the beam section. It should be noted that the maximum value of M_b is M_y, beyond which the plastic hinge will appear and the curvature within the length of the beam will no longer maintain a linear distribution.

$$\theta_1 = \frac{M_b l_b}{3EI_b} \tag{8}$$

The rotation value θ_2 was calculated by the two-stage bond-slip model proposed by Sezen and Setzler [23,24], as shown in Figure 6. When the concrete strain was ignored, the development length L_d can be solved by the equilibrium condition of the axial tension and bond forces of the reinforcement. Then, the amount of slip s of the steel bars was obtained by Formula (9). Using the two-stage strain distribution model in Figure 6, Formula (9) can be expressed in the form of Formula (10), where d is the diameter of the steel bars. Since the depth x of the compression zone of the beam end in each loading phase was accurately solved, θ_2 was calculated by Formula (11), where a_s is the edge distance of steel bars ($a_{s,top}$ or $a_{s,bot}$).

$$s = \int_0^{L_d} \varepsilon_s dx \tag{9}$$

$$s = \begin{cases} \frac{\varepsilon_s \sigma_s d}{8\sqrt{f_c}} \varepsilon_s \leq \varepsilon_y \\ \frac{\varepsilon_y f_y d}{8\sqrt{f_c}} + \frac{(\varepsilon_s + \varepsilon_y) d (\sigma_s - f_y)}{4\sqrt{f_c}} \varepsilon_s > \varepsilon_y \end{cases} \tag{10}$$

$$\theta_2 = \frac{s}{h_b - a_s - x} \tag{11}$$

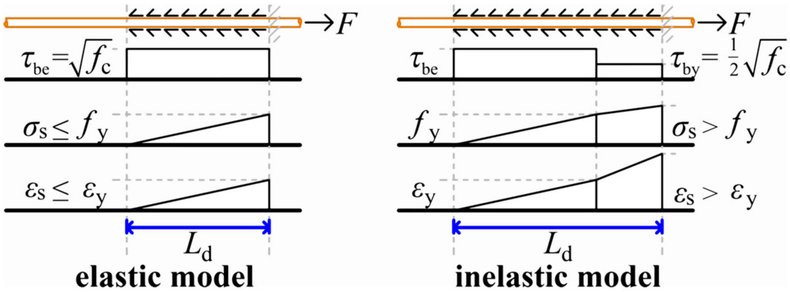

Figure 6. The two-stage bond-slip model, adapted from ref. [23].

Assuming that the length of plastic hinge was $h_b/2$ and that the curvature within this range was uniform [25,26], the maximum curvature ϕ_{max} was obtained by strain distribution on the beam section at the interface of the beam and the column:

$$\phi_{max} = \frac{\varepsilon_s}{h_b - a_s - x} \quad (12)$$

The curvature ϕ_{max} here can be considered as the superposition of the uniform curvature within the range of the plastic hinge and the yield curvature ϕ_y. Thus, the rotation value θ_3 can be obtained by the following formula:

$$\theta_3 = \left(\phi_{max} - \phi_y\right)\frac{h_b}{2} \quad (13)$$

The rotation value θ_4 was the ratio of the sum of flexural deformation of the upper and lower columns and the total height, as shown in the following formula, where M_c is the maximum moment of the column, l_c is the clear height of the column, and EI_c is the flexural rigidity of columns.

$$\theta_4 = \frac{2}{3} \cdot \frac{M_c {l_c}^2}{(2l_c + h_b)EI_c} \quad (14)$$

2.3. Construction of Moment–Rotation Relationship

For T-shaped exterior beam–column connections, some of θ_1–θ_4 will contribute to the total deformation for each calculated characteristic moment value. The θ values of each moment were added up for the corresponding column rotation. Therefore, the four required characteristic points can be obtained in both positive and negative directions. For example, the result of the positive direction was similar to the dashed line in Figure 1. Since there is only one beam in a T-shaped connection, the cumulative method is applicable to both symmetric and asymmetric reinforced beams.

However, for cruciform interior beam–column connections, beams on the left and right sides of the column do not crack, yield, or fail simultaneously in case of asymmetrical reinforcement or different concrete strengths on the upper and lower beam sections (such as the commonly used laminated beams). This is because the mechanical behaviors of the positive and negative directions of the beam are different, but the beams on both sides of the column need to satisfy the deformation compatibility condition. Therefore, a two-step calculation method is proposed in this section, as shown in Figure 7. In step 1, since the effect of beam deformation on column rotation θ_1–θ_3 is a series system, the moment–rotation behavior of the beam at one side can be obtained by superposition. The superposition results are controlled by four points in both positive and negative directions, respectively (the positive result of one beam is like the heavy line of step 1 in Figure 7). In step 2, considering the deformation compatibility of the beams on the left and right sides (marked as beam 1 and beam 2 in Figure 7), the total M–θ curve (marked as sum result in Figure 7) controlled by 7 points (the beam that was destroyed first represents the failure of the entire joint) can be obtained by summing the M–θ curves of the beams on left and right sides calculated from step 1. The result of this operation is approximate because the control points of the same beam (the solid lines of beam 1 and beam 2 in step 2) do not strictly satisfy the linear relationship. Then, the final result can be obtained by superposing θ_4 on the sum result and considering the influence of the P-Δ effect $(M - P\theta(2l_c + h_b))$. Here, M is the total moment, and P is the axial force at the top of the column. The shear behavior of the core zone can also be adopted in step 2 if it is a vital component.

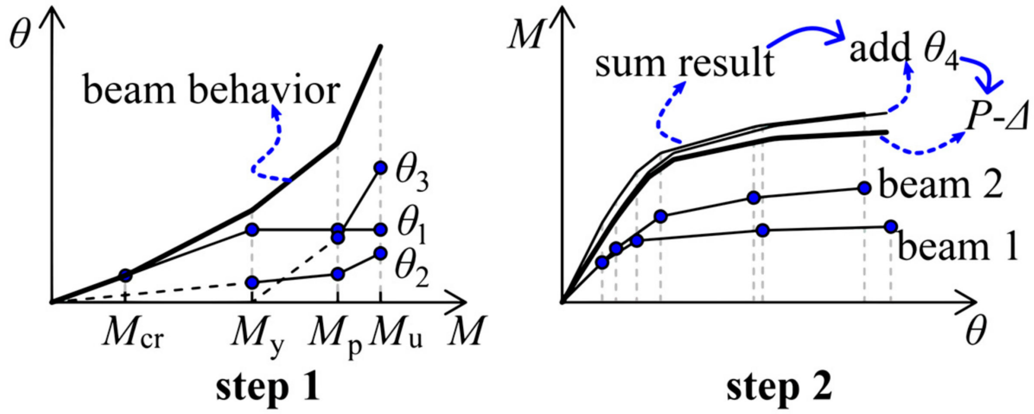

Figure 7. Calculation method of moment–rotation relationship for cruciform connections.

3. Test Database

A total of 17 low-cyclic loading tests of MPBC connections in recent years (in the last five years) were selected for the quantification of the moment–rotation relationship. A total of 76 specimens, including 58 precast connections and 18 cast-in situ counterparts, were selected from these tests. Almost all the precast connections have their counterparts, so the comparison between them is appropriate. These tested beam–column connections are empty frames, excluding floor slabs and filler walls. In the form, there are T-shaped exterior connections, cruciform interior connections, and L-shaped top connections, covering almost all forms of the beam–column connections of the frame structures. These specimens follow the principle of "strong columns and weak beams, strong joints and weak members", and their reported failure modes were basically controlled by the flexural failure of beams. Therefore, the calculation method in this paper can basically represent all the loading and deformation characteristics of the connections.

Due to different configurations, the selected precast specimens were classified into five categories, as shown in Table 1. The basis for such classifications was the position of the post-casting concrete and the anchorage position and anchorage methods of the steel bars. Differences in these two aspects between connections in different categories can be seen in the descriptions and connection details in Table 1. The reason for such classification is that, due to the use of the fine fiber section analysis method, the range and strength of post-casting concrete will affect the definition of fibers. If the plastic hinge regions at the beam ends are completely cast-in situ (type 4 and type 5), the strength characteristics of the concrete fibers are only affected by a constrained effect; if the areas are layered (type 1–3), the strength difference between old and new concrete is taken into account when defining the material properties. Similarly, the connecting methods of the beam longitudinal bars will directly affect the use of steel bars in the calculation processes. Beam longitudinal bars in different categories used for analysis were highlighted in the connection details. The configurations of these five types of beam–column connections are broadly representative, and basically cover those of the existing MPBC connections.

Table 1. Information of selected specimens.

Type	Researchers	Specimens	Descriptions	Connection Details
Type 1	Lee et al. [27] (2017) Gou et al. [28] (2018) Hou et al. [29] (2018) Zhao et al. [30] (2019) Zhang et al. [31] (2020)	A2, A3, B2, B3 P-RC, P-ECC1–5 YKJ-1, YKJ-2 PK-1–4 P-HUPC1–4	(1) Post-casting concrete in the core zone and on the upper beam. (2) Beam bottom bars protrude into the core zone for anchorage.	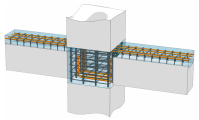
Type 2	Guan et al. [32] (2018) Guerrero et al. [33] (2019) Yang et al. [34] (2019) Lin et al. [35] (2021)	S2, S3 Specimen 2–4 SP-1–4 PU-30, PU-45, PU-80	(1) Post-casting concrete in the U-shaped keyway, on the upper beam, and in the core zone. (2) Beam bottom bars protrude into the core zone for anchorage.	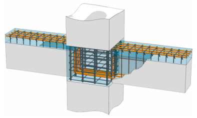
Type 3	Liu et al. [36] (2019) Gou et al. [37] (2019)	JC40, JC45, JC50 PU-ECC1–4	(1) Post-casting concrete in the U-shaped keyway, on the upper beam, and in the core zone. (2) Beam bottom bars do not protrude into the core zone; additional bars are used for lapping in the keyway.	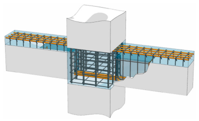
Type 4	Wahjudi et al. [38] (2015) Feng et al. [39] (2018) Yan et al. [4] (2018)	BCC Type 2–5 PJZ-1–2 P1–5	(1) Post-casting concrete at the beam end; the core zone is prefabricated. (2) Beam bars and re-bars protruding from the core zone are mechanically connected or lapped in post-casting areas.	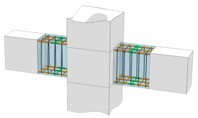
Type 5	Lu et al. [40] (2018) Yan et al. [41] (2018) Ghayeb et al. [42] (2020)	JMC3, JME3, JSC2, JSC4, JSE2 PPCJ1~2 PRCC	(1) Post-casting concrete at the beam end, on the upper beam, and in the core zone. (2) Beam bottom bars do not protrude into the core zone; additional bars are used for lapping in beam ends.	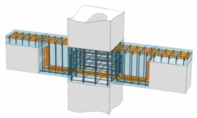

Four parameters, including the concrete strength f_c (prism strength), the diameter of beam longitudinal bars d, the yield strength of beam longitudinal bars f_y, and the clear span–depth ratio of the beams $2l_b/h_b$, of the selected 76 specimens were counted, as shown in Figure 8. This shows that f_c is mainly distributed in 30–60 MPa, d in 16–25 mm, and f_y in 400–500 MPa, and the span–depth ratio of the beams is about eight. These parameters can accurately reflect the material types and member sizes commonly used in engineering.

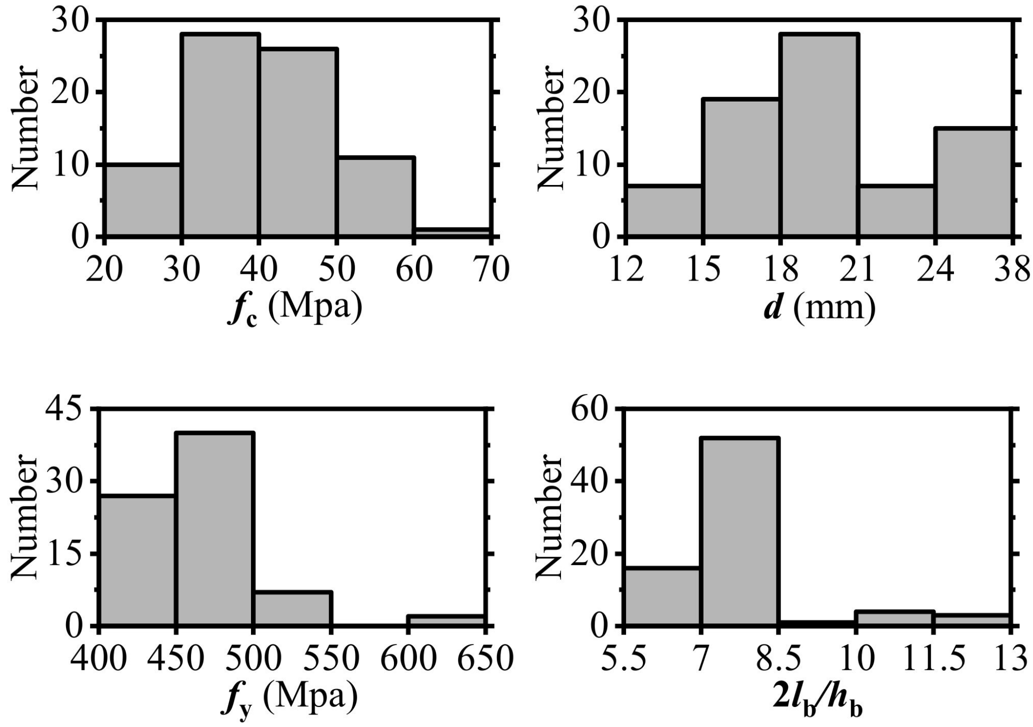

Figure 8. Parameter statistics of the selected specimens.

4. Quantification Results

The moment–rotation curves of all the MPBC connections and the corresponding cast-in situ connections in Table 1 were calculated according to the proposed method in Section 2. Two loading patterns, including loading at the column top and anti-symmetric loading at beam ends, were applied in these tests. For verification with the test results, the relative rotation of columns and beams was calculated, respectively, to correspond to the loading patterns. When the mechanical behaviors of the left and right beams of the interior joints are different (as with beam 1 and beam 2 in Figure 7), there are seven characteristic points on the curves in positive and negative directions, respectively. That is, there are two results for the cracking points, yield points, and peak points in each direction (the two results represent the same state of beams on both sides). The cracking point and yield point with larger ratios and the peak point with larger moments were selected as the characteristic points of the joint to quantify the relevant parameters of the moment–rotation relationship. Figure 9 shows the quantification results of each characteristic point based on the calculated values. Solid points are the results of cast-in situ connections, and hollow points are the results of precast connections. Values on the *x*-axis are the test rotation of the corresponding characteristic points. Values on the *y*-axis are the ratio of calculated values and test values. Two statistical parameters, mean and standard deviation, were identified in Figure 9. The mean value was used to quantify the difference of characteristic point parameters between cast-in situ connections and MPBC connections, and the standard deviation was used to verify the accuracy of the proposed method. Although the number of cast-in situ connections and precast connections is different, almost all precast specimens have their counterparts. Additionally, their calculation method was the same. Therefore, the comparison between them is reliable.

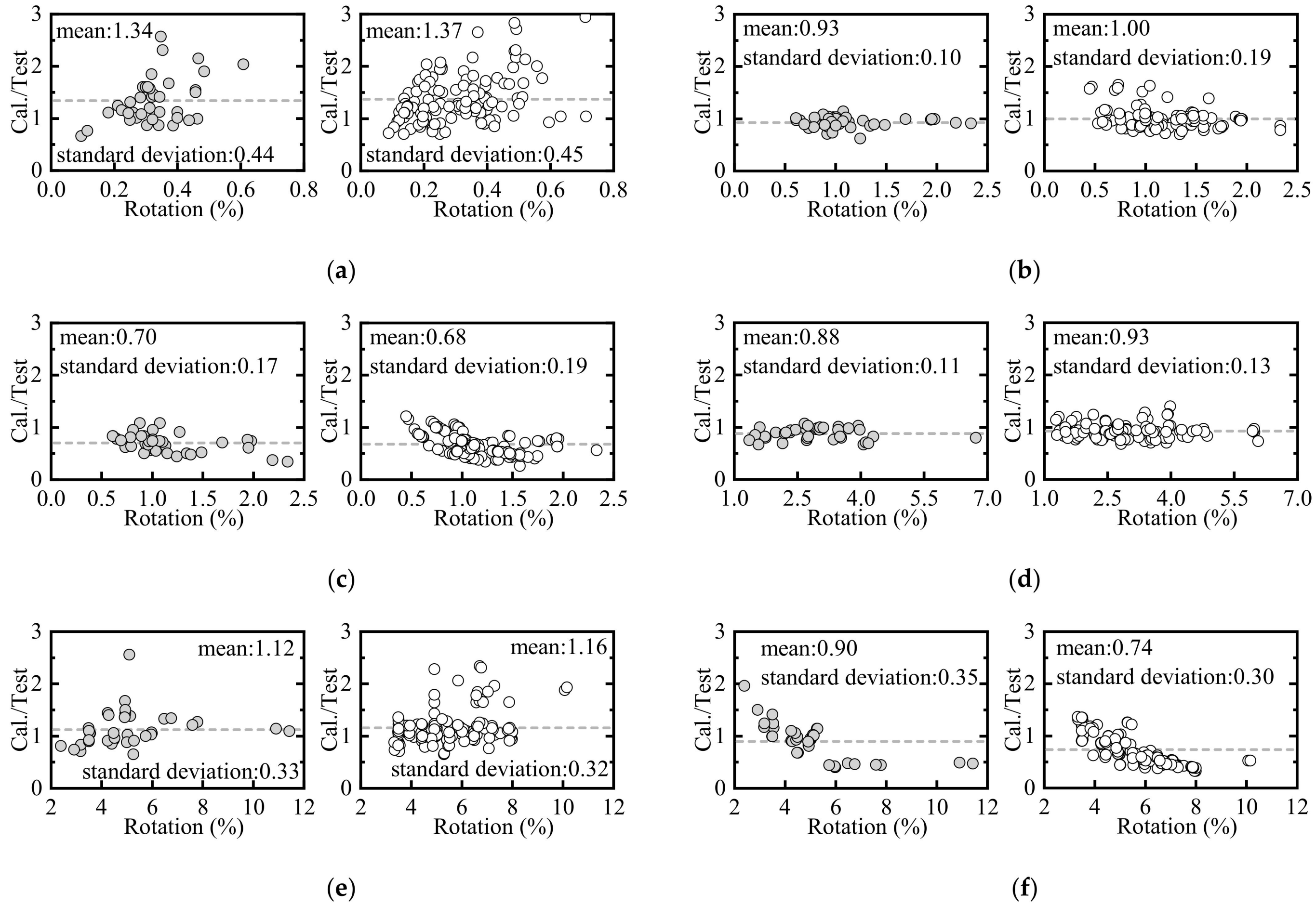

Figure 9. Quantification of each characteristic point of the moment–rotation relationship based on calculation results. Note: The solid points are the results of cast-in situ connections, the hollow points are the results of MPBC connections, and the dashed lines are the mean lines. (**a**) Comparison of initial stiffness; (**b**) Comparison of M_y; (**c**) Comparison of θ_y; (**d**) Comparison of M_p; (**e**) Comparison of M_u; (**f**) Comparison of θ_u.

Because of the small change of stiffness at the initial stage of cracking, it is difficult to accurately determine the cracking point. Therefore, the initial stiffness, characterizing the structural behavior before cracking, was analyzed, as shown in Figure 9a. The initial stiffness values are discrete after quantification since the results are densely distributed between 0.5 and 2.0. The quantitative mean values of cast-in situ and precast connections are 1.34 and 1.37, respectively, indicating that the calculated stiffness is larger than tested. This phenomenon is predictable because the elastic stiffness is sensitive to the mounting errors of the loading devices in tests. In addition, the stiffness of specimens in the positive and negative directions is usually different, because the initial loading damage often leads to the reduction of the stiffness in the other direction. Nevertheless, it can be found that their mean values are very close, and their standard deviations are almost the same. Therefore, we can conclude that the initial stiffness is consistent between MPBC connections and cast-in situ connections. For the yield points (Figure 9b,c), the standard deviations of the moment (0.10, 0.19) and rotation (0.17, 0.19) are acceptable after quantification. In terms of the mean values, precast joints have smaller yield moments and larger relative rotation (higher mean values indicate smaller experimental values), suggesting that the pre-yield stiffness of MPBC connections is smaller. For peak points, Figure 9d shows that the calculated peak moment is also highly reliable (standard deviations are only 0.11, 0.13), and the moment of precast joints is slightly lower. The rotation values of peak points were not quantified, because the stiffness of beams after yielding is small and the displacements of these points are of little significance to structural analysis [12]. For ultimate points (Figure 9e,f), the quantification results are more discrete compared to those of yield points and peak points, because the nonlinearity of joints is extremely high and the destruction of joints is controlled by various mechanisms. The quantified ultimate moment values are similar (1.12 and 1.16, respectively), but the rotation of precast connections is larger. Therefore, there is no need to worry about the insufficient ductility of MPBC connections. In addition, it is noted that the data set in Figure 9f is negatively sloped, which is not parallel to the horizontal line, where the mean is. This is determined by the relatively conservative calculation method of ultimate points in this paper. Of course, it can be seen from the horizontal axis that the failure rotation of most tested specimens is greater than 4%, which has far exceeded the requirements in the current code [43]. Therefore, the smaller estimate of the large displacement value is acceptable, since the application scenarios in that state are very limited.

The modification coefficient of each quantification parameter of MPBC connections was obtained by dividing the mean value of the corresponding quantification parameter of the cast-in situ joints by that of the precast joints (see Figure 9), and the modification coefficients of six parameters are listed in Table 2. If the modification coefficient is greater than 1, the relevant parameter would be modified to a larger value. Overestimating the ductility and bearing capacity of joints will reduce the design requirements, resulting in unsafe design results. The modifications that deviate from conservation design concepts are regarded as favorable factors, and, vice versa, are unfavorable factors. Based on the principle of "considering unfavorable factors and ignoring favorable factors" in engineering design, the modification of θ_u can be ignored. The modification coefficient of K_1 is close to 1, and this coefficient can also be neglected considering the error interference of statistical samples. Although the coefficient (0.96) of M_u is unfavorable, the ultimate moment values of precast joints are the result of larger displacements and, thus, can also be ignored. Therefore, the modifications to the yield moment, yield rotation, and peak moment of the MPBC connections can be adopted when they are designed based on the equivalent cast-in situ method.

Table 2. Modification coefficients from quantification.

Relevant Parameters	Modification Coefficients	Adopted or Not
K_1	0.98	No
M_y	0.93	Yes
θ_y	1.03	Yes
M_p	0.95	Yes
M_u	0.96	No
θ_u	1.22	No

All calculated moment–rotation curves and the corresponding test results were compared. Two typical results with good prediction and two typical results with poor prediction are presented in Figure 10, respectively. The figure also illustrates the contribution value of each deformation mechanism of the beams and the column when loading in positive and negative directions to the total rotation. As is shown, before yielding, the flexural deformation of beams is the main rotation source, and after yielding, the beam hinge deformation is the main rotation source. Despite some differences in bearing capacity and stiffness deviations, it can still be considered that the proposed calculation method is suitable for predicting the moment–rotation relationship of MPBC connections.

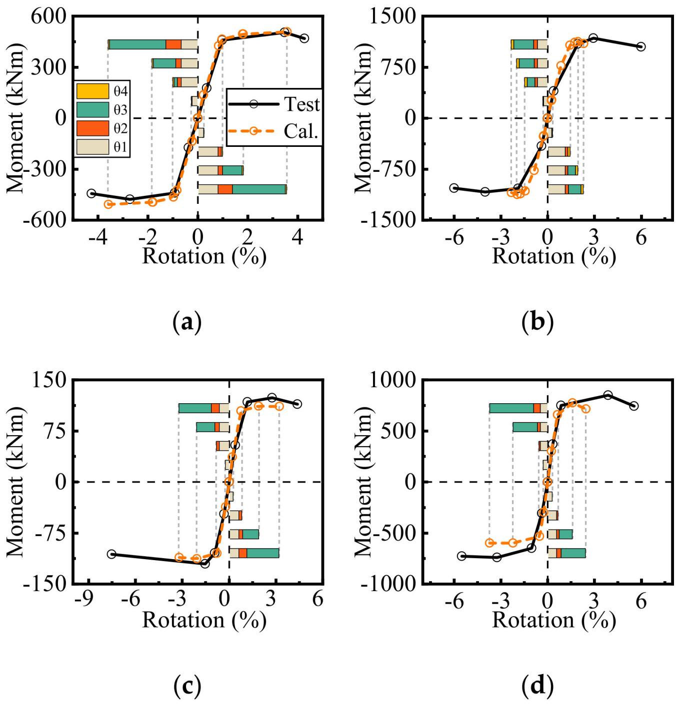

Figure 10. Comparison of prediction and test results of moment–rotation curves. (**a**) S2 adapted from ref. [32]; (**b**) A2 adapted from ref. [27]; (**c**) P-ECC2 adapted from ref. [28]; (**d**) Specimen 3 adapted from ref. [33].

5. Conclusions

A great concern of designers in recent years is whether the traditional section analysis method of cast-in situ connections can be directly used for the design and analysis of MPBC connections. Given the complexity of local configurations of MPBC connections, the fine fiber section analysis method was used and the confined effect of stirrups was considered for moment and strain computation. Moreover, four mechanisms affecting the joint deformation were taken into account and a two-step construction method was proposed for solving the deformation compatibility of beams. Therefore, the method for calculating four-linear idealized M–θ curves of MPBC connections was formed. In order to verify the accuracy of the proposed method and quantify the characteristic point parameters, the moment–rotation curves of 58 commonly used MPBC connections and their 18 cast-in situ counterparts were calculated. The main conclusions are as follows:

(1) The proposed calculation method for the moment–rotation relationship is suitable for both MPBC connections and cast-in situ connections. The bearing capacity and deformation capacity of beam–column connections can be well predicted by this method;

(2) The accuracy of the moment–rotation relationship between cast-in situ connections and MPBC connections calculated by this method is highly consistent and satisfactory. Therefore, the deformation mechanisms considered in this paper are sufficient to reflect the deformation sources of beam–column connections, and there is no need to consider new participation components when calculating the deformation of MPBC connections;

(3) The quantification results suggest that the yield strength, peak strength, and pre-yield stiffness of MPBC connections are smaller than those of cast-in situ connections, and modifications to them can be adopted during design. The ductility of MPBC connections is sufficient. There is no need to modify their ultimate bearing capacity and ultimate displacement during calculation or analysis.

There are still some shortages in this study, which need to be further investigated in the future. Since the shear deformation of the core zone was not considered, the beam–column joints for calculation need to be designed by the principle of "strong columns and weak beams, strong joints and weak members"; that is, the joints are finally destroyed by the flexural failure of beams. The calculation method in this paper is not appropriate for joints of shear failure. When calculating the relative slip of steel bars, it was defaulted that the anchorage length of steel bars with different anchorage methods was sufficient; that is, the pullout failure mode of re-bars was not considered.

Author Contributions: Conceptualization, B.S. and W.X.; methodology, W.X.; software, B.S.; validation, B.S. and W.X.; formal analysis, D.D.; investigation, B.S.; resources, D.D.; data curation, W.X.; writing—original draft preparation, B.S.; writing—review and editing, W.X. and D.D.; visualization, B.S.; supervision, S.W.; project administration, S.W.; funding acquisition, D.D. and S.W. All authors have read and agreed to the published version of the manuscript.

Funding: This research was funded by the National Natural Science Foundation of China, grant numbers 51678302, 51808291; Six Talent Peaks Project in Jiangsu Province, grant number JY-022.

Institutional Review Board Statement: Not applicable.

Informed Consent Statement: Not applicable.

Data Availability Statement: Not applicable.

Conflicts of Interest: The authors declare no conflict of interest.

References

1. Fan, J.J.; Wu, G.; Feng, D.C.; Zeng, Y.H.; Lu, Y. Seismic performance of a novel self-sustaining beam-column connection for precast concrete moment-resisting frames. *Eng. Struct.* **2020**, *222*, 111096. [CrossRef]
2. Wang, H.; Marino, E.M.; Pan, P.; Liu, H.; Nie, X. Experimental study of a novel precast prestressed reinforced concrete beam-to-column joint. *Eng. Struct.* **2018**, *156*, 68–81. [CrossRef]
3. Parastesh, H.; Hajirasouliha, I.; Ramezani, R. A new ductile moment-resisting connection for precast concrete frames in seismic regions: An experimental investigation. *Eng. Struct.* **2014**, *70*, 144–157. [CrossRef]
4. Yan, Q.; Chen, T.; Xie, Z. Seismic experimental study on a precast concrete beam-column connection with grout sleeves. *Eng. Struct.* **2018**, *155*, 330–344. [CrossRef]
5. Lu, Z.; Huang, J.; Dai, S.; Liu, J.; Zhang, M. Experimental study on a precast beam-column joint with double grouted splice sleeves. *Eng. Struct.* **2019**, *199*, 109589. [CrossRef]
6. Fan, J.J.; Feng, D.C.; Wu, G.; Hou, S.; Lu, Y. Experimental study of prefabricated RC column-foundation assemblies with two different connection methods and using large-diameter reinforcing bars. *Eng. Struct.* **2020**, *205*, 110075. [CrossRef]
7. Ketiyot, R.; Hansapinyo, C. Seismic performance of interior precast concrete beam-column connections with T-section steel inserts under cyclic loading. *Earthq. Eng. Eng. Vib.* **2018**, *17*, 355–369. [CrossRef]
8. Senturk, M.; Pul, S.; Ilki, A.; Hajirasouliha, I. Development of a monolithic-like precast beam-column moment connection: Experimental and analytical investigation. *Eng. Struct.* **2020**, *205*, 110057. [CrossRef]
9. Feng, S.; Guan, D.; Guo, Z.; Liu, Z.; Li, G.; Gong, C. Seismic performance of assembly joints between HSPC beams and concrete-encased CFST columns. *J. Constr. Steel Res.* **2021**, *180*, 106572. [CrossRef]
10. MHURD-PRC (Ministry of Housing and Urban-Rural Development of the People's Republic of China). *Code for Design of Concrete Structures (GB50010)*; MHURD-PRC: Beijing, China, 2010. (In Chinese)
11. MHURD-PRC (Ministry of Housing and Urban-Rural Development of the People's Republic of China). *Technical Specification for Precast Structures (JGJ 1-2014)*; MHURD-PRC: Beijing, China, 2010. (In Chinese)
12. Birely, A.C.; Lowes, L.N.; Lehman, D.E. A model for the practical nonlinear analysis of reinforced-concrete frames including joint flexibility. *Eng. Struct.* **2012**, *34*, 455–465. [CrossRef]
13. Alva, G.; Debs, A. Moment–rotation relationship of RC beam-column connections: Experimental tests and analytical model. *Eng. Struct.* **2013**, *56*, 1427–1438. [CrossRef]
14. Rasulo, A.; Pelle, A.; Lavorato, D.; Fiorentino, G.; Nuti, C.; Briseghella, B. Finite element analysis of reinforced concrete bridge piers including a flexure-shear interaction model. *Appl. Sci.* **2020**, *10*, 2209. [CrossRef]
15. Amaris, A.; Pampanin, S.; Palermo, A. Uni and bi-directional quasi static tests on alternative hybrid precast beam column joint subassemblies. In Proceedings of the New Zealand Society for Earthquake Engineering Conference, Christchurch, New Zealand, 13–15 April 2006; pp. 1–8.
16. Pampanin, S.; Priestley, M.J.N.; Sritharan, S. Analytical modelling of the seismic behaviour of precast concrete frames designed with ductile connections. *J. Earthq. Eng.* **2001**, *5*, 329–367. [CrossRef]
17. Guan, D.; Guo, Z.; Xiao, Q.; Zheng, Y. Experimental study of a new beam-to-column connection for precast concrete frames under reversal cyclic loading. *Adv. Struct. Eng.* **2016**, *19*, 529–545. [CrossRef]
18. Xue, W.; Bai, H.; Dai, L.; Hu, X.; Dubec, M. Seismic behavior of precast concrete beam-column connections with bolt connectors in columns. *Struct. Concr.* **2021**, *22*, 1297–1314. [CrossRef]

19. Feng, P.; Qiang, H.L.; Ye, L.P. Discussion and definition on yield points of materials, members and structures. *Eng. Mech.* **2017**, *34*, 36–46.
20. Park, R.; Priestley, M.; Gill, W.D. Ductility of square-confined concrete columns. *J. Struct. Div.* **1982**, *108*, 929–950. [CrossRef]
21. Elmorsi, M.; Kianoush, M.R.; Tso, W.K. Nonlinear analysis of cyclically loaded reinforced concrete structures. *ACI Struct. J.* **1998**, *95*, 725–739.
22. General Administration of Quality Supervision, Inspection and Quarantine of the People's Republic of China. *Steel for the Reinforcement of Concrete—Part 2: Hot Rolled Ribbed Bars (GB/T 1499.2)*; General Administration of Quality Supervision, Inspection and Quarantine of the People's Republic of China: Beijing, China, 2018. (In Chinese)
23. Sezen, H.; Setzler, E.J. Reinforcement slip in reinforced concrete columns. *ACI Struct. J.* **2008**, *105*, 280–289.
24. Feng, D.C.; Gang, W.; Yong, L. Finite element modelling approach for precast reinforced concrete beam-to-column connections under cyclic loading. *Eng. Struct.* **2018**, *174*, 49–66. [CrossRef]
25. Park, H.; Eom, T. A simplified method for estimating the amount of energy dissipated by flexure-dominated reinforced concrete members for moderate cyclic deformations. *Earthq. Spectra* **2006**, *22*, 459–490. [CrossRef]
26. Eom, T.S.; Park, H.G. Evaluation of energy dissipation of slender reinforced concrete members and its applications. *Eng. Struct.* **2010**, *32*, 2884–2893. [CrossRef]
27. Lee, H.J.; Chen, H.C.; Syu, J.H. Seismic performance of emulative precast concrete beam–column connections with alternative reinforcing details. *Adv. Struct. Eng.* **2017**, *20*, 136943321769363. [CrossRef]
28. Gou, S.; Ding, R.; Fan, J.; Nie, X.; Zhang, J. Seismic performance of a novel precast concrete beam-column connection using low-shrinkage engineered cementitious composites. *Constr. Build. Mater.* **2018**, *192*, 643–656. [CrossRef]
29. Hou, G.; Wang, X.; Lu, N.; Xie, J.; Huang, G. Experimental study on seismic behavior of new prefabricated partial SRC frame beam-column joints. *Build. Struct.* **2018**, *48*, 27–32.
30. Zhao, Y.; Li, Y.; Bi, Q.; Deng, S. Experimental investigation on seismic performance of knee joints for monolithic precast concrete frame. *J. Tongji Univ. Nat. Sci.* **2019**, *47*, 600–608.
31. Zhang, Z.Y.; Ding, R.; Nie, X.; Fan, J. Seismic performance of a novel interior precast concrete beam-column joint using ultra-high performance concrete. *Eng. Struct.* **2020**, *222*, 111145. [CrossRef]
32. Guan, D.; Jiang, C.; Guo, Z.; Ge, H. Development and seismic behavior of precast concrete beam-to-column connections. *J. Earthq. Eng.* **2018**, *22*, 234–256. [CrossRef]
33. Guerrero, H.; Rodriguez, V.; Escobar, J.A.; Alcocera, S.M.; Bennetts, F.; Suarez, M. Experimental tests of precast reinforced concrete beam-column connections. *Soil Dyn. Earthq. Eng.* **2019**, *125*, 105743. [CrossRef]
34. Yang, H.; Guo, Z.; Yin, H.; Guan, D.; Yang, S. Development and testing of precast concrete beam-to-column connections with high-strength hooked bars under cyclic loading. *Adv. Struct. Eng.* **2019**, *22*, 3042–3054. [CrossRef]
35. Lin, Y.; Chen, Z.; Guan, D.; Guo, Z. Experimental study on interior precast concrete beam-column connections with UHPC core shells. *Structures* **2021**, *32*, 1103–1114. [CrossRef]
36. Liu, Y.; Cai, J.; Deng, X.; Cao, Y.; Feng, J. Experimental study on effect of length of service hole on seismic behavior of exterior precast beam-column connections. *Struct. Concr.* **2019**, *20*, 85–96. [CrossRef]
37. Gou, S.; Ding, R.; Fan, J.; Nie, X. Experimental study on seismic performance of precast LSECC/RC composite joints with U-shaped LSECC beam shells. *Eng. Struct.* **2019**, *189*, 618–634. [CrossRef]
38. Wahjudi, D.I.; Suprobo, P.; Sugihardjo, H.; Tavio. Performance of precast reinforced concrete beam-to-column subassemblages with connection constructed out of The Panel. *Aust. J. Basic Appl. Sci.* **2015**, *9*, 111–121.
39. Feng, B.; Xiong, F.; Chen, J.; Chen, W.; Zhang, Y. Effects of postcast connection locations on the seismic performance of precast concrete frame joints. *Struct. Des. Tall Spec. Build.* **2018**, *27*, e1544. [CrossRef]
40. Lu, C.; Dong, B.; Pan, J.; Shan, Q.; Hanif, A.; Yin, W. An investigation on the behavior of a new connection for precast structures under reverse cyclic loading. *Eng. Struct.* **2018**, *169*, 131–140. [CrossRef]
41. Yan, X.; Wang, S.; Huang, C.; Qi, A.; Hong, C. Experimental study of a new precast prestressed concrete joint. *Appl. Sci.* **2018**, *8*, 1871. [CrossRef]
42. Ghayeb, H.H.; Razak, H.A.; Sulong, N.H.R. Seismic performance of innovative hybrid precast reinforced concrete beam-to-column connections. *Eng. Struct.* **2020**, *202*, 109886. [CrossRef]
43. MHURD-PRC (Ministry of Housing and Urban-Rural Development of the People's Republic of China). *Code for Seismic Design of Buildings (GB50011)*; MHURD-PRC: Beijing, China, 2010. (In Chinese)